A Bidirectional Three-Phase Push–Pull Converter With Dual Asymmetrical PWM Method

Minho Kwon, Junsung Park, and Sewan Choi, *Senior Member, IEEE*

***Abstract*—This paper proposes a new bidirectional three-phase push–pull converter that has a simple structure and achieves zero-voltage switching turn-on of switches. Also, due to use of a single inductor, an imbalance among phase currents on the low-voltage high-current side is trivial in the proposed converter although no current sharing control is employed. In this paper, a new dual asymmetrical pulse width modulation (PWM) switching method is proposed for bidirectional power flow control with seamless mode change. The proposed switching method offers reduced circulating current and makes the converter easier to implement compared to the PWM plus phase shift-based control method since it is a general PWM method having two independent duty cycle controls on each side. Experimental results from a 3-kW prototype are provided to validate the proposed concept.**

***Index Terms*—Bidirectional dc–dc converter, push–pull, three-phase.**

I. Introduction

RECENTLY, high-power bidirectional dc–dc converters (BDCs) have aroused much interest in many applications such as energy storage systems, uninterruptible power supplies, solid-state transformers, electric vehicles, etc.

In particular, isolated BDCs have been used for the applications where bidirectional power flow with high-voltage step-up ratio and/or galvanic isolation is required, and a variety of topologies with high-frequency transformers have been proposed in [1]–[10]. BDCs based on flyback converters [1]–[3] can achieve soft-switching and clamping of surge voltage using auxiliary components. The power density can be improved in some low-power applications. But they are not suitable for high-power application due to stored energy in the transformer. A dual active bridge (DAB) converter [11] has symmetric structure and can achieve zero-voltage switching (ZVS) without using auxiliary components. However, the converter has a limited ZVS range and high circulating currents under wide voltage variation. In order to overcome the problems, many advanced modulation strategies for the DAB converter have been presented [12]–[18]. The most serious problem associated with the low impedance nature of the voltage-fed converter is that the magnetic core saturation that can be caused by a possible flux imbalance may lead to switch failure. A BDC based on dual half-bridge converters [5] has halved the component count compared to the dual full-bridge topologies and guarantees volt–sec balance of the transformer. By controlling two control variables of duty and phase, current stresses on the switching devices and transformer could be kept minimum. However, large current rating of capacitors is an obstacle to selection of proper capacitors in high-power applications.

In order to overcome the problem associated with high device stresses when implemented with the single-phase dc–dc converter mentioned above, the three-phase dc–dc converter has been introduced in high-power applications [11], [19]–[36].

Generally, the three-phase dc–dc converter has several advantages over its single-phase counterpart: easy switch selection due to reduced current rating, reduction of the input and output filters' volume due to increased effective switching frequency by a factor of three, and reduction in transformer size due to better transformer utilization [27].

A three-phase DAB converter [11], [20], [29] has basically voltage-fed natures on both low-voltage side (LVS) and high-voltage side (HVS). The three-phase DAB converter also suffers from issues on narrow ZVS region, increased circulating current under wide voltage range operation, and magnetic core saturation of the transformer as the single-phase DAB converter does. A phase-shift three-phase bidirectional series-resonant converter [33] processes power in a sinusoidal manner and achieves soft switching, and therefore, the switching losses and noise can be significantly reduced. However, a tolerance of the resonant elements could be an impediment to high volume production of the converter.

The PWM plus phase shift (PPS) method [6] has been applied to the three-phase BDC based on the current-fed converter on the LVS and the voltage-fed converter on the HVS [34], [35]. The converter has several advantages such as minimized RMS values of current in switches and transformers, maintainable ZVS conditions over a wide range, and free direction change of the power flow. However, possible three-phase currents imbalance on the low-voltage high-current side due to tolerance of three inductors could be a challenging issue since it may cause overrating of switches, magnetic core saturation, and unequal thermal distribution, especially at high-power applications. A sophisticated control strategy has been proposed for balancing the three-phase inductor currents [37], making the controller to be complicated.

In this paper, a three-phase push–pull BDC with active clamping is proposed for high-power applications. The features of the proposed converter are as follows:

Manuscript received December 10, 2014; revised March 2, 2015; accepted April 23, 2015. Date of publication May 8, 2015; date of current version November 16, 2015. This work was supported by the National Research Foundation of Korea grant funded by the Korea government (2014R1A2A2A01003724). Recommended for publication by Associate Editor D. Xu.

M. Kwon and S. Choi are with the Department of Electrical and Information Engineering, Seoul National University of Science and Technology, Seoul 139-743, Korea (e-mail: saemnae@seoultech.ac.kr; schoi@seoultech.ac.kr).

J. Park is with the Department of New Energy Engineering, Seoul National University of Science and Technology, Seoul 139-743, Korea (e-mail: pjs09507@seoultech.ac.kr).

Color versions of one or more of the figures in this paper are available online at http://ieeexplore.ieee.org.

Digital Object Identifier 10.1109/TPEL.2015.2431273

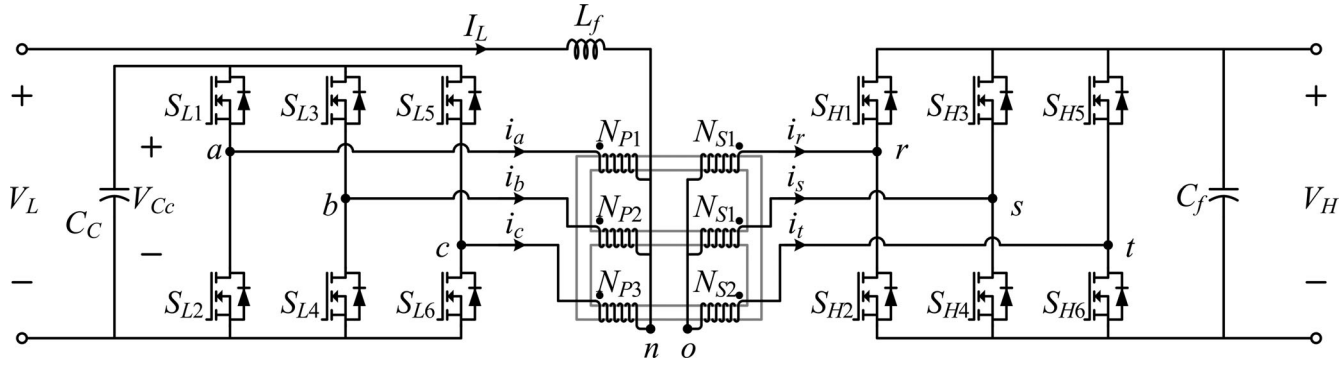

Fig. 1. Proposed bidirectional three-phase push–pull converter.

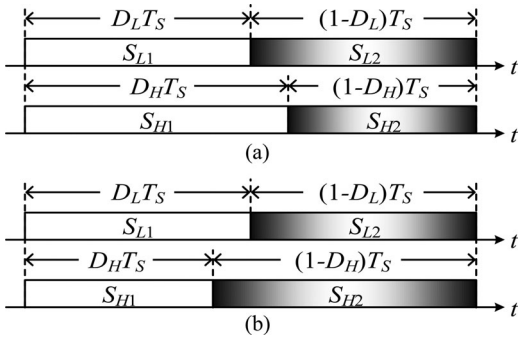

Fig. 2. Switching pattern of the DAPWM. (a) Boost operation. (b) Buck operation.

1) owing to inherent boost characteristics, the turn-ratio of the transformer can be reduced and the current ripple on the LVS is small;
2) the circulating current can be reduced by regulating the capacitor voltage on the LVS;
3) the magnetic core saturation caused by flux imbalance of the transformer is greatly relieved due to high impedance nature at the current-fed side [38];
4) no current-sharing control is needed since imbalance among phase currents on the low-voltage high-current side is trivial.

Also, a new dual asymmetrical pulse width modulation (DAPWM) switching method is proposed for bidirectional power flow control with seamless mode change. Further, owing to the use of two independent duty cycles, circulating currents can be reduced by matching the primary voltage with the secondary voltage referred to the primary. Besides, the proposed DAPWM method is easier to implement compared to the PPS method since it is a general PWM method having two independent duty cycle controls on each side.

II. Proposed Converter

The proposed converter is basically a three-phase current-fed push–pull converter with active clamp [27], as shown in Fig. 1. The LVS of the proposed converter includes a three-phase switch bridge consisting of six switches $S_{L1} - S_{L6}$, clamp capacitor C_C, and input filter inductor L_f which is operated at three times the switching frequency. The HVS of the proposed converter is a three-phase switch bridge consisting of six switches $S_{H1} - S_{H6}$. The three-phase windings of the transformer are configured in *Y–Y* connection. The neutral point of the three-phase primary winding is connected to the input source through the input filter inductor. Note that a three-leg core must be used for proper operation of the proposed converter.

A. Switching Method

Fig. 2 shows the switching pattern of the proposed DAPWM method for a phase of the converter. Two control variables, D_L and D_H, are used for both forward (boost) and reverse (buck) operation. Duty cycles, D_L and $1 - D_L$, of the top and bottom switches of the LVS are used to maintain constant capacitor voltage V_{Cc} under varying LVS voltage condition. The voltage across C_c is determined by following equation:

$$V_{Cc} = \frac{V_L}{D_L}. \tag{1}$$

In the meanwhile, duty cycles, D_H and $1 - D_H$, of the top and bottom switches of the HVS are used to control the power flow between the LVS and HVS. The direction of power flow is determined by relative magnitude of the two duty cycles: $D_L < D_H$ for boost operation and $D_L > D_H$ for buck operation. The three switch pairs are interleaved with 120° phase shift, which leads to an increased effective switching frequency, thereby reducing input-current ripple.

B. Operating Principles

In this section, the operating principles of the boost and buck operations of the proposed converter are described in detail. The key waveforms and operation stages of the proposed converter for boost operation are shown in Figs. 3 and 4, respectively. The behavior of the converter in the one-third switching cycle can be described by three stages. Fig. 5 shows simplified equivalent circuits of each stage for detailed circuit analysis. For the sake of simplicity, it is assumed that the controlled voltage across C_C is equal to V_H/N, where *N* is turn ratio of transformer(N_S/N_P),

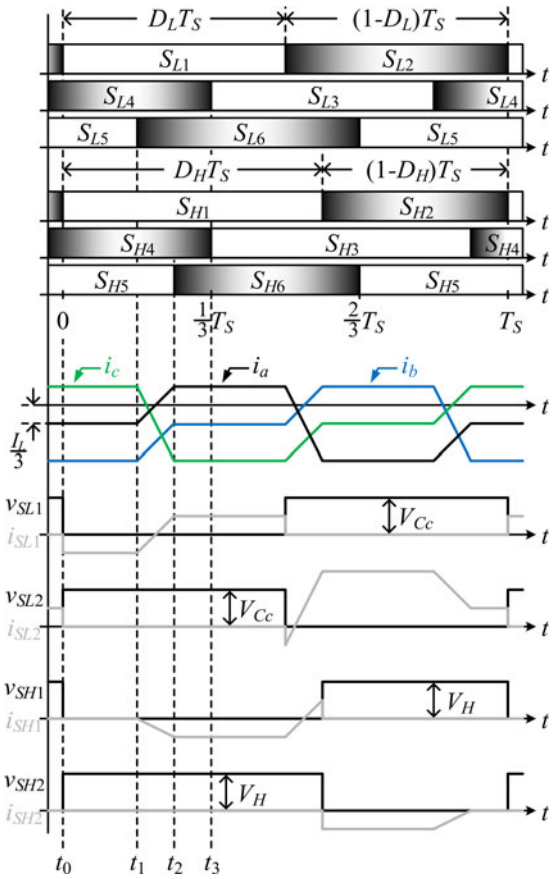

Fig. 3. Key waveforms of the proposed converter with DAPWM (boost operation).

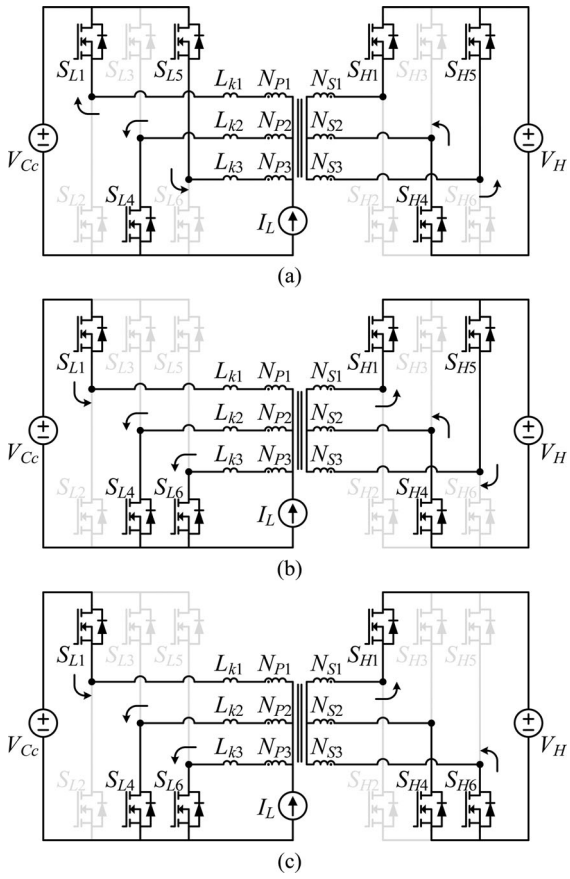

Fig. 4. Operation stages of the proposed converter (boost operation). (a) $t_0 - t_1$. (b) $t_1 - t_2$. (c) $t_2 - t_3$.

the current through L_f is constant during the switching period T_S, and leakage inductances of each phase are L_k.

Stage I [t_0–t_1]: Before t_0, switches S_{L2}, S_{L4}, S_{L5}, S_{H2}, S_{H4}, and S_{H5} are being turned ON. At t_0, switches S_{L2} and S_{H2} are turned OFF, and switches S_{L1} and S_{H1} are turned ON, which causes changes in the voltages across the leakage inductors and the voltage can be obtained from Fig. 5(a). Thus, the slopes of the phase currents flowing through the leakage inductors can be expressed as follows:

$$\frac{di_a}{dt} = \frac{di_c}{dt} = \frac{NV_{Cc} - V_H}{3NL_k} \tag{2}$$

$$\frac{di_b}{dt} = \frac{2(V_H - NV_{Cc})}{3NL_k}. \tag{3}$$

Because V_{Cc} is equal to V_H/N, the slopes of each current flowing through the leakage inductors are zero, meaning all the phase current are constant in this stage. During this stage, the power is transferred from LVS to HVS. At HVS, the current flows only through S_{H4} and S_{H5}, although switch S_{H1} is being turned ON. Note that S_{L1} is turned ON under ZVS condition, and the ZVS current is the same as phase current $i_a(t_1) = -I_L/3$.

Stage II [t_1–t_2]: At t_1, switch S_{L5} is turned OFF, and S_{L6} is turned ON under ZVS condition. It can be seen from Fig. 5(b) that i_c starts to decrease with the slope which is determined by

$$\frac{di_c}{dt} = \frac{-NV_{Cc} - V_H}{3NL_k}. \tag{4}$$

As i_c decreases, phase currents i_a and i_b increase with the slopes determined, respectively, by

$$\frac{di_a}{dt} = \frac{2NV_{Cc} - V_H}{3NL_k} \tag{5}$$

$$\frac{di_b}{dt} = \frac{-NV_{Cc} + 2V_H}{3NL_k}. \tag{6}$$

Stage III [t_2–t_3]: At t_2, switch S_{H5} is turned OFF, and S_{H6} is turned ON under ZVS condition. The slopes of the phase currents can be obtained from Fig. 5(c) as follows:

$$\frac{di_a}{dt} = \frac{2(NV_{Cc} - V_H)}{3NL_k} \tag{7}$$

$$\frac{di_b}{dt} = \frac{di_c}{dt} = \frac{-NV_{Cc} + V_H}{3NL_k}. \tag{8}$$

All the phase currents are constant because V_{Cc} is equal to V_H/N. This is the power transfer mode such as *Stage I*. At HVS, the current flows only through S_{H1} and S_{H6} although S_{H4} is being turned ON. At t_3, switches S_{L4} and S_{H4} are turned OFF, and S_{L3} and S_{H3} are turned ON. Note that switches S_{H3} is turned ON and S_{H4} is turned OFF under ZCS condition,

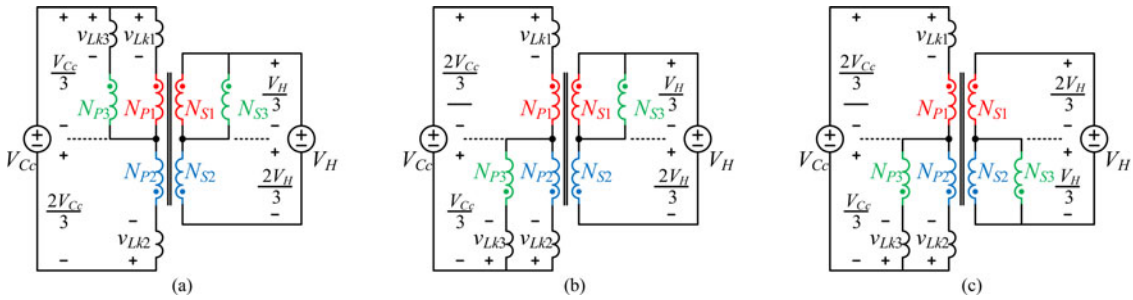

Fig. 5. Equivalent circuit for each mode (boost operation). (a) $t_0 - t_1$. (b) $t_1 - t_2$. (c) $t_2 - t_3$.

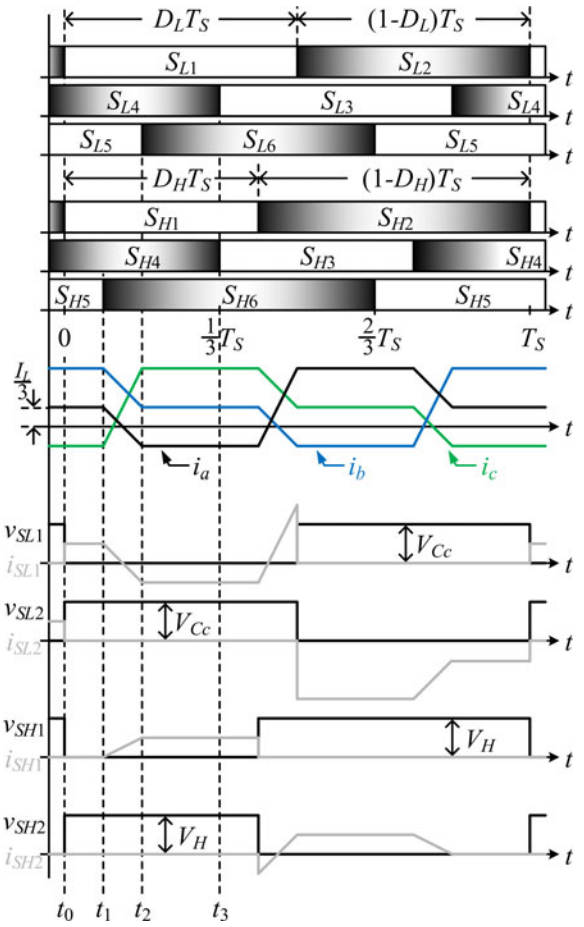

Fig. 6. Key waveforms of the proposed converter with DAPWM (buck operation).

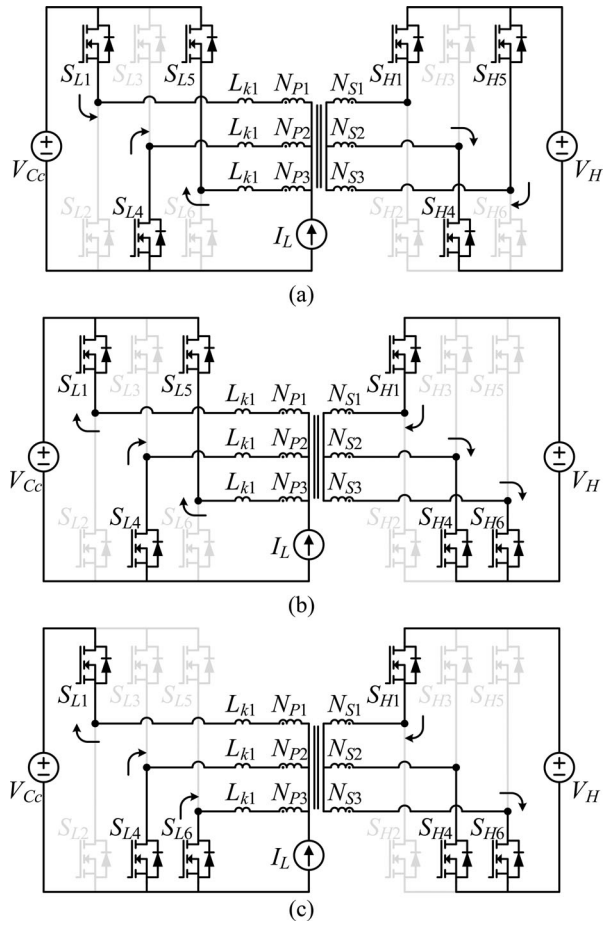

Fig. 7. Operation stages of the proposed converter (buck operation). (a) $t_0 - t_1$. (b) $t_1 - t_2$. (c) $t_2 - t_3$.

respectively. The rest of the switching cycle is repetition of these operation stages.

The key waveforms and operation stages of the proposed converter for buck operation are shown in Figs. 6 and 7. In the buck operation, the proposed converter with DAPWM method has three operating stages within a one-third switching cycle. Detailed explanation of operating stages is omitted here since the operating principle of the buck operation is very similar to the boost operation.

C. ZVS Condition

Most of the switches of the proposed converter achieve soft-switching except for LVS top switches in buck mode. Tables I and II show the switching characteristics and ZVS currents of the switches, respectively. Fig. 8 shows the ZVS regions of both LVS and HVS bottom switches under LVS voltage variation.

TABLE I
SWITCHING CHARACTERISTIC OF THE PROPOSED CONVERTER

	Boost mode	Buck mode
LVS top switches	ZVS turn-on	Hard switching
LVS bottom switches	ZVS turn-on	ZVS turn-on
HVS top switches	ZCS turn-on	ZCS turn-on
HVS bottom switches	ZVS turn-on & ZCS turn-off	ZVS turn-on & ZCS turn-off

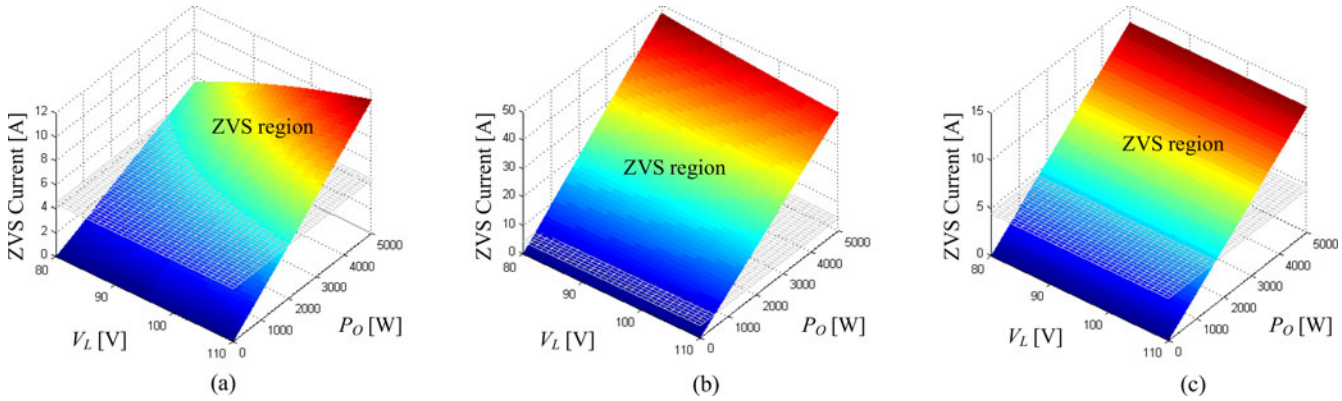

Fig. 8. ZVS currents of the bottom switches ($V_H = 380$ V, $L_k = 3\ \mu$H, $N = 2$, $f_s = 50$ kHz, and $C_{oss} = 1650$ pF). (a) LVS in boost mode. (b) LVS in buck mode. (c) HVS in boost and buck mode.

TABLE II
ZVS CURRENTS OF THE SWITCHES

	Boost mode	Buck mode
LVS top switches	$-\frac{I_L}{3}$	–
LVS bottom switches	$\frac{-I_L}{3} + \frac{V_H(D_H - D_L)}{3Nf_sL_k}$	$\frac{I_L}{3} - \frac{V_H(D_H - D_L)}{3Nf_sL_k}$
HVS top switches	–	–
HVS bottom switches	$-\frac{V_H(D_H - D_L)}{3f_sL_kN^2}$	$-\frac{V_H(D_H - D_L)}{3f_sL_kN^2}$

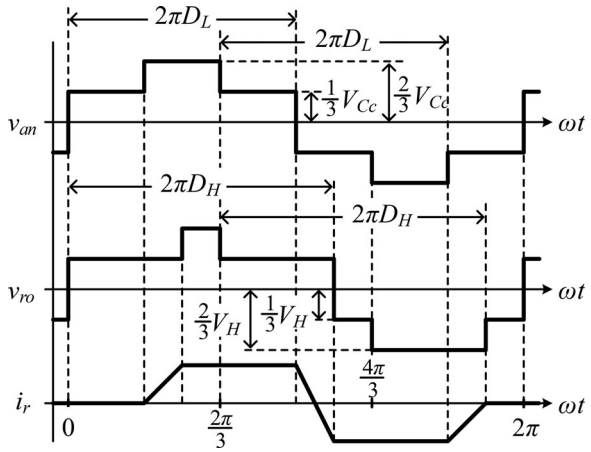

Fig. 9. Waveforms of winding voltage and current for obtaining power equation.

D. Power Equation

Fig. 9 shows waveforms of the winding voltage and current for obtaining power equation of the proposed converter assuming $V_{Cc} = V_H/N$. The power equation of DAPWM method can be obtained by the integration of the instantaneous power over one switching period

$$P_O = \frac{3}{T_S}\int_0^{T_S} v_{ro}(t) i_r(t) dt \tag{9}$$

where v_{ro} is the instantaneous voltage across N_{S1}, and the secondary current i_r is

$$i_r(t) = \frac{N v_{an}(t) - v_{ro}(t)}{N^2 L_k} \cdot t + i_r(0) \tag{10}$$

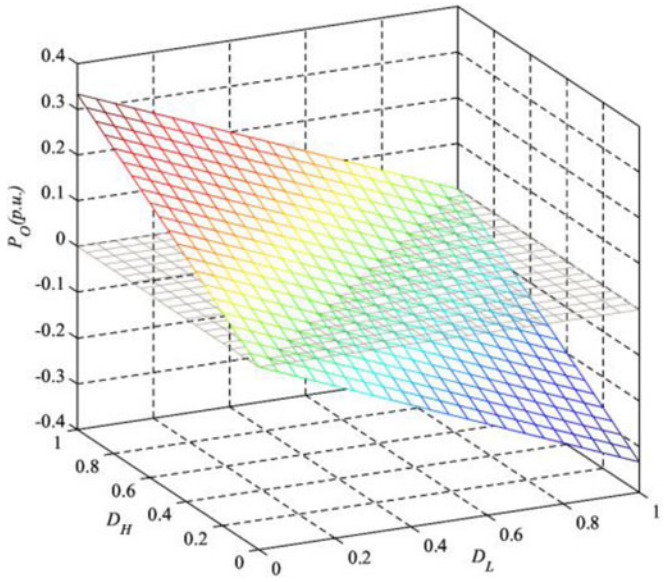

Fig. 10. Power flow versus D_H and D_L.

where $i_r(0) = 0$ and v_{an} is the instantaneous voltage across N_{P1}. The power equation can be obtained from (9) and (10) by

$$P_O = \frac{V_H^2(D_H - D_L)}{3f_S L_k N^2} \tag{11}$$

where f_S is the switching frequency of the proposed converter. The normalized power equation can be expressed as follows:

$$P_{O(p.u)} = \frac{D_H - D_L}{3} \tag{12}$$

where $1\,\text{p.u.} = V_H^2/(f_s L_k N^2)$. Using (12), the power flow of the proposed converter as a function of D_H and D_L is plotted as shown in Fig. 10.

E. Control Strategy

Two control variables, D_H and D_L, are used to control not only power flow but voltage across C_c. Therefore, circulating current can be reduced by matching voltage across C_c with the secondary voltage referred to the primary. Fig. 11 shows the control block diagram of the proposed converter for bidirectional

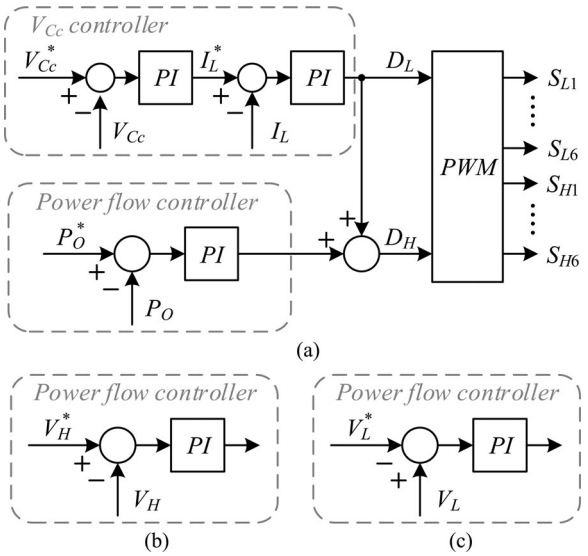

Fig. 11. Control block diagram of the proposed converter for bidirectional operation. (a) Whole control block diagram with output power regulation. (b) Power flow controller by HVS voltage regulation. (c) Power flow controller by LVS voltage regulation.

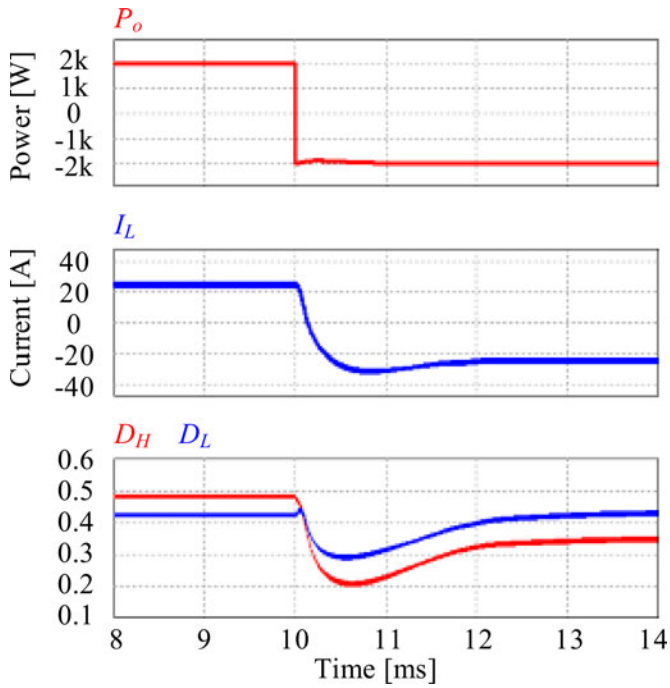

Fig. 12. Simulation waveforms showing seamless mode transfer under step power flow reversal.

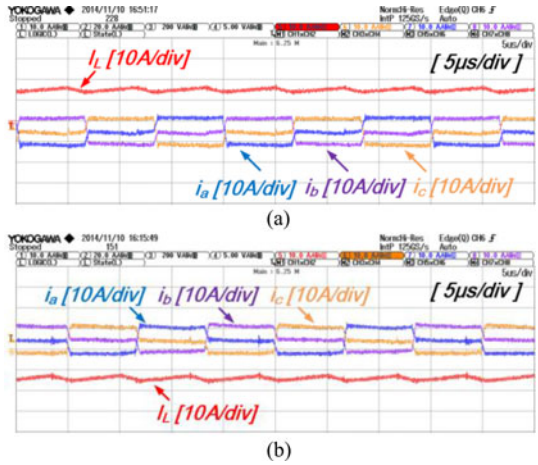

Fig. 13. Experimental waveforms of the primary phase currents. (a) Boost mode. (b) Buck mode.

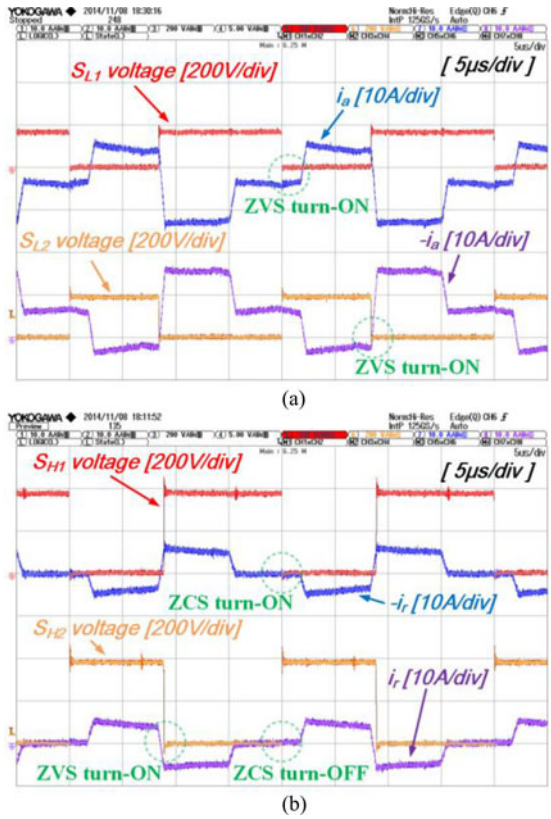

Fig. 14. Experimental waveforms of switch voltages and current in boost mode. (a) LVS. (b) HVS.

operation. Fig. 11(a) shows the whole control block diagram consisting of the clamp capacitor voltage(V_{Cc}) controller and the power flow controller. In order to match the voltage across C_c with HVS voltage referred to primary side, the reference value of V_{Cc} is determined as follows:

$$V_{Cc}^* = \frac{V_H}{N}. \tag{13}$$

V_{Cc} controller was implemented using an average current-mode controller. D_L is the output of V_{Cc} controller. D_H is determined by adding D_L to the output of the power flow controller. A positive output of the power flow controller makes D_H be greater than D_L, leading the converter to operate in boost mode. On the other hand, a negative output of the power flow controller makes D_L greater than D_H, leading the converter to operate in buck mode. The power flow controller can also be implemented with either HVS voltage regulation, as shown in Fig. 11(b), or LVS voltage regulation, as shown in Fig. 11(c).

Fig. 12 shows simulation waveforms illustrating the performance of the proposed closed-loop system. Note that the

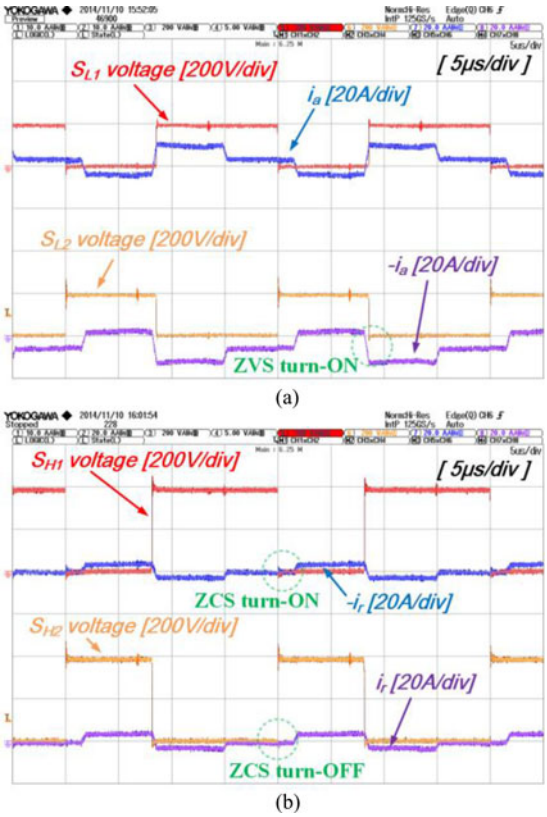

Fig. 15. Experimental waveforms of switch voltages and current in buck mode. (a) LVS. (b) HVS.

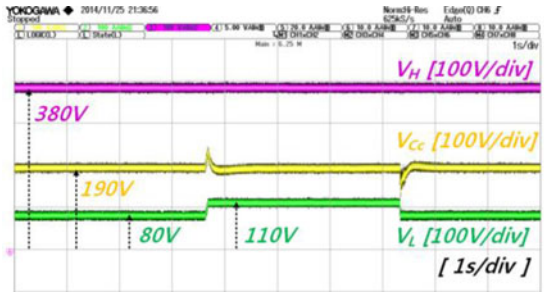

Fig. 16. Experimental waveforms under LVS voltage variation.

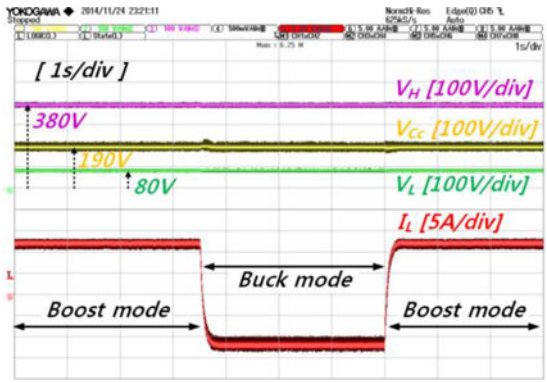

Fig. 17. Experimental waveforms under power flow change.

converter is operating under the worst case operating condition of step power flow reversal. During the boost operation, D_H is greater than D_L. It should be noted that after step power flow reversal, D_H decreases smoothly and becomes smaller than D_L.

III. Experimental Results

To verify the operating principle of the proposed converter, a 3-kW prototype was built according to the following specification: $P_o = 3$ kW, $V_H = 380$ V, $N = 2$, $V_L = 80 - 110V$, $f_s = 50$ kHz, $L_k = 3$ μH, $\Delta I_L = 6$ A, and $\Delta V_{Cc} = 2$ V.

The current ripple of L_f and the voltage ripple of C_c can be obtained as follows:

$$\Delta I_L = \frac{V_H \cdot (D_L^2 - D_L + 2/9)}{N \cdot L_f \cdot f_s} \tag{14}$$

$$\Delta V_{Cc} = \frac{2/3 - D_L}{3 \cdot C_c \cdot f_s} \cdot \left(\frac{P_O \cdot N}{V_H \cdot D_L} - \frac{V_H (D_H - D_L)}{N \cdot L_k \cdot f_s} \right). \tag{15}$$

Using (14) and (15), the inductance and the capacitance of the prototype are calculated as $L_f = 18$ μH and $C_C = 10$ μF. Considering some margin, actual values of $L_f = 20$ μH and $C_C = 18$ μF were used, respectively. Both LVS and HVS switches are implemented with IXFN110N60P3 (600 V, 110 A, and 56 mΩ) MOSFET. An off-the-shelf EI core of the ferrite material is used for the three-phase transformer. Unidentical leakage and magnetizing inductances of each phase of the transformer may cause imbalance in three-phase currents. In order to reduce the imbalance, mismatch in leakage and magnetizing inductances of each phase of the transformer should be made as small as possible. Since the cross-sectional area of the center leg of the core is twice them of the both side legs, the center leg is cut out so as to have equal width [25]. Fig. 13 shows the primary phase current waveforms and interleaved current $I_{\rm L}$. Note that imbalance among the phase currents is hardly seen even though no current sharing control is employed in the experiment. Figs. 14 and 15 show the experimental waveforms of the boost and buck operations of the proposed converter, respectively. It can be seen that switches are turned ON under ZVS(ZCS) and/or turned OFF under ZCS. Figs. 16 and 17 demonstrate regulation performances under voltage variation and power flow change, respectively. Fig. 16 shows that V_{Cc} is well regulated under step changes in LVS voltage. Fig. 17 shows that I_L is smoothly changing under step changes in P_O^*. The measured efficiencies for the boost and buck modes are shown in Fig. 18. The measured efficiency in the buck mode is lower than that in the boost mode because the LVS top switches are turned ON with hard-switching in the buck mode, while all switches achieve ZVS or ZCS turn-on in the boost mode. The efficiency was measured using Yokogawa WT3000. The maximum efficiencies of the boost and buck modes are 96% at 2.5 kW and 95.4% at 3 kW, respectively. Fig. 19 shows the photograph of the proposed converter.

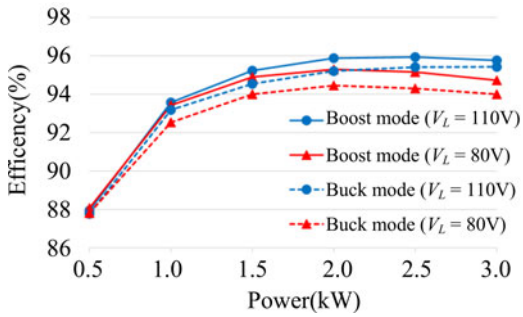

Fig. 18. Measured efficiency as a function of the output power.

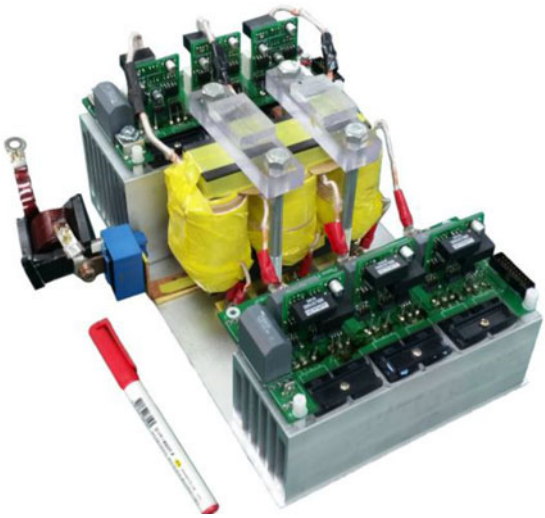

Fig. 19. Photograph of the proposed converter prototype.

IV. Conclusion

In this paper, a new bidirectional three-phase push–pull converter with active clamp that helps achieve not only clamping of surge voltage but soft switching of switches has been proposed. Due to high impedance nature at LVS of the proposed converter, the magnetic core saturation of the transformer is negligible, which makes the proposed converter viable for higher power application.

The proposed DAPWM technique for the bidirectional three-phase push–pull converter provides the following advantages: identical switching patterns of boost and buck modes leads to seamless mode change under power flow reversal; circulating currents are reduced by matching the primary voltage with the secondary voltage referred to the primary; and the conventional PWM technique can be employed unlike the PPS method where both phase-shift angle and duty cycle should be controlled, thereby allowing simple implementation. A 3-kW prototype of the proposed converter has been built and tested to verify the validity of the proposed operation. Imbalance among the phase currents has hardly been observed even though no current sharing control is employed in the experiment. The maximum efficiencies measured in the boost and buck modes are 96% at 2.5 kW and 95.4% at 3 kW, respectively. According to the results, the proposed converter could be a promising candidate for high-power isolated dc–dc converter system where bidirectional power flow is required.

References

[1] G. Chen, Y. Lee, S. Y. R. Hui, and D. Xu, "Actively clamped bidirectional flyback converter," *IEEE Trans. Ind. Electron.*, vol. 47, no. 4, pp. 770–779, Aug. 2000.

[2] H. S. Chung, W. Cheung, and K. S. Tang, "A ZCS bidirectional flyback DC/DC converter," *IEEE Trans. Power Electron.*, vol. 19, no. 6, pp. 1426–1434, Nov. 2004.

[3] W. Li, H. Wu, H. Yu, and X. He, "Isolated winding-coupled bidirectional ZVS converter with PWM plus phase-shift (PPS) control strategy," *IEEE Trans. Power Electron.*, vol. 26, no. 12, pp. 3560–3570, Dec. 2011.

[4] H. Xiao and S. Xie, "A ZVS bidirectional DC–DC converter with phase-shift plus PWM control scheme," *IEEE Trans. Power Electron.*, vol. 23, no. 2, pp. 813–823, Mar. 2008.

[5] F. Z. Peng, H. Li, G. Su, and J. S. Lawler, "A new ZVS bidirectional DC–DC converter for fuel cell and battery application," *IEEE Trans. Power Electron.*, vol. 19, no. 1, pp. 54–65, Jan. 2004.

[6] D. Xu, C. Zhao, and H. Fan, "A PWM plus phase-shift control bidirectional DC–DC converter," *IEEE Trans. Power Electron.*, vol. 19, no. 3, pp. 666–368, May 2004.

[7] S. Inoue and H. Akagi, "A bidirectional DC–DC converter for an energy storage system with galvanic isolation," *IEEE Trans. Power Electron.*, vol. 22, no. 6, pp. 2299–2306, Nov. 2007.

[8] Z. Zhang, Z. Ouyang, O. C. Thomsen, and M. A. E. Andersen, "Analysis and design of a bidirectional isolated DC–DC converter for fuel cells and supercapacitors hybrid System," *IEEE Trans. Power Electron.*, vol. 27, no. 2, pp. 848–859, Feb. 2012.

[9] Z. Zhang, O. C. Thomsen, and M. A. E. Andersen, "Optimal design of a push-pull-forward half-bridge (PPFHB) bidirectional DC–DC converter with variable input voltage," *IEEE Trans. Ind. Electron.*, vol. 59, no. 7, pp. 2761–2771, Jul. 2012.

[10] P. Xuewei and A. K. Rathore, "Naturally clamped zero-current commutated soft-switching current-fed push–pull DC/DC converter: analysis, design, and experimental results," *IEEE Trans. Power Electron.*, vol. 33, no. 3, pp. 1318–1327, Mar. 2015.

[11] R. W. De Doncker, D. M. Divan, and M. H. Kheraluwala, "A three-phase soft-switched high-power-density dc/dc converter for high-power applications," *IEEE Trans. Ind. Appl.*, vol. 27, no. 1, pp. 63–73, Jan./Feb. 1991.

[12] H. Bai and C. Mi, "Eliminate reactive power and increase system efficiency of isolated bidirectional dual-active-bridge DC–DC converters using novel dual-phase-shift control," *IEEE Trans. Power Electron.*, vol. 23, no. 6, pp. 2905–2914, Nov. 2008.

[13] A. K. Jain and R. Ayyanar, "PWM control of dual active bridge: comprehensive analysis and experimental verification," *IEEE Trans. Power Electron.*, vol. 26, no. 4, pp. 1215–1227, Nov. 2011.

[14] G. G. Oggier, G. O. Garcia, and A. R. Oliva, "Modulation strategy to operate the dual active bridge DC–DC converter under soft switching in the whole operating range," *IEEE Trans. Power Electron.*, vol. 26, no. 4, pp. 1228–1236, Nov. 2011.

[15] F. Krismer and J. W. Kolar, "Closed form solution for minimum conduction loss modulation of DAB converters," *IEEE Trans. Power Electron.*, vol. 27, no. 1, pp. 174–188, Jan. 2012.

[16] B. Zhao, Q. Song, W. Liu, and W. Sun, "Current-stress-optimized switching strategy of isolated bidirectional DC–DC converter with dual-phase-shift control," *IEEE Trans. Power Electron.*, vol. 60, no. 10, pp. 4458–4467, Oct. 2013.

[17] D. Jeong, M. Ryu, H. Kim, and H. Kim, "Optimized design of bidirectional dual active bridge converter for low-voltage battery charger," *J. Power Electron.*, vol. 14, no. 3, pp. 468–477, May 2014.

[18] H. Wen and B. Su, "Reactive power and soft-switching capability analysis of dual-active-bridge dc-dc- converters with dual-phase-shift control," *J. Power Electron.*, vol. 15, no. 1, pp. 18–30, Man. 2015.

[19] A. R. Prasad, P. D. Ziogas, and S. Manias, "Analysis and design of a three-phase off-line dc-dc converter with high frequency isolation," *IEEE Trans. Ind. Appl.*, vol. 27, no. 4, pp. 824–832, Jul./Aug. 1992.

[20] G. Su and L. Tang, "A three-phase bidirectional DC-DC converter for automotive applications," in *Proc. IEEE Ind. Appl. Soc. Annu. Meet.*, Oct. 2008, pp. 1–7.

[21] C. Liu, A. Johnson, and J. Lai, "A novel three-phase high-power soft-switched DC/DC converter for low-voltage fuel cell applications," *IEEE Trans. Ind. Appl.*, vol. 41, no. 6, pp. 1691–1697, Nov./Dec. 2005.
[22] D. S. Oliveira Jr., F. L. M. Antunes, and C. E. A. Silva, "A three-phase ZVS PWM DC–DC converter associated with a double-wye connected rectifier, delta primary," *IEEE Trans. Power Electron.*, vol. 21, no. 6, pp. 1684–1690, Nov. 2007.
[23] H. Cha, J. Choi, and P. N. Enjeti, "A three-phase current-fed DC-DC converter with active clamp for low-DC renewable energy sources," *IEEE Trans. Power Electron.*, vol. 23, no. 6, pp. 2784–2793, Nov. 2008.
[24] R. L. Andersen and I. Barbi, "A three-phase current-fed push-pull dc-dc converter," *IEEE Trans. Power Electron.*, vol. 24, no. 2, pp. 358–368, Feb. 2009.
[25] J. A. Garcia and G. Moon, "A high-efficiency three-phase ZVS PWM converter utilizing a positive double-star active rectifier stage for server power supply," *IEEE Trans. Power Ind. Electron.*, vol. 58, no. 8, pp. 3317–3329, Feb. 2011.
[26] S. V. G. Oliveira and I. Barbi, "A three-phase step-up DC–DC converter with a three-phase high-frequency transformer for DC renewable power source applications," *IEEE Trans. Power Ind. Electron.*, vol. 58, no. 8, pp. 3567–3580, Feb. 2011.
[27] S. Lee, J. Park, and S. Choi, "A three-phase current-fed push-pull DC-DC converter with active clamp for fuel cell applications," *IEEE Trans. Power Electron.*, vol. 26, no. 8, pp. 2266–2277, Aug. 2011.
[28] P. Xuewei, U. R. Prasanna, and A. K. Rathore, "Magnetizing-inductance-assisted extended range soft-switching three-phase AC-link current-fed DC/DC converter for low DC voltage applications," *IEEE Trans. Power Electron.*, vol. 28, no. 7, pp. 3317–3328, Jul. 2013.
[29] S. P. Engel, N. Soltau, H. Stagge, and R. W. De Doncker, "Improved instantaneous current control for high-power three-phase dual-active bridge DC–DC converters," *IEEE Trans. Power Electron.*, vol. 29, no. 8, pp. 4067–4077, Aug. 2014.
[30] Y. Hu, W. Xiao, W. Li, and X. He, "Three-phase interleaved high-step-up converter with coupled-inductor-based voltage quadrupler," *IET Power Electron.*, vol. 7, no. 7, pp. 1841–1849, Jul. 2014.
[31] S. S. Tanavade, H. M. Suryawanshi, K. L. Thakre, and M. A. Chaudhari, "Application of three-phase resonant converter in high power DC supplies," *IEE Proc. Electric Power Appl.*, vol. 125, no. 6, pp. 1401–1409, Nov. 2005.
[32] M. S. Almardy and A. K. S. Bhat, "Three-phase (LC)(L)-type series-resonant converter with capacitive output filter," *IEEE Trans. Power Electron.*, vol. 26, no. 4, pp. 1172–1183, Apr. 2011.
[33] R. Mirzahosseini and F. Tahami, "A phase-shift three-phase bidirectional series resonant dc/dc converter," in *Proc. 37th Annu. Conf. IEEE Electron. Soc.*, Nov. 2011, pp. 1137–1134.
[34] H. Cha, J. Choi, and B. Han, "A new three-phase interleaved isolated boost converter with active clamp for fuel cells," in *Proc. IEEE Power Electron. Spec. Conf.*, Jun. 2008, pp. 1271–1276.
[35] Z. Wang and H. Li, "A soft switching three-phase current-fed bidirectional DC-DC converter with high efficiency over a wide input voltage range," *IEEE Trans. Power Electron.*, vol. 27, no. 2, pp. 669–684, Feb. 2012.
[36] S. Bal, A. K. Rathore, and D. Srinivasan, "Modular snubberless bidirectional soft-switching current-fed dual 6-pack (CFD6P) DC/DC converter," *IEEE Trans. Power Electron.*, vol. 33, no. 2, pp. 519–523, Feb. 2015.
[37] Z. Wang and H. Li, "Three-phase bidirectional DC-DC converter with enhanced current sharing capability," in *Proc. IEEE Energy Convers. Congr. Expo.*, Atlanta, GA, USA, Sep. 2010, pp. 1116–1122.
[38] A. I. Pressman, K. Billings, and T. Morey, "Current-mode and current-fed topologies," in *Switching Power Supply Design*, 3th ed. New York, NY, USA: McGraw-Hill 2007, pp. 161–227.

Minho Kwon was born in Korea, in 1985. He received the B.S. and M.S. degrees from the Department of Control and Instrumentation Engineering, Seoul National University of Science and Technology, Seoul, Korea, in 2012 and 2014, respectively, where he is currently working toward the Ph.D. degree at the Power Electronics and Fuel Cell power Conditioning Laboratory.

His research interests include bidirectional dc–dc converter and grid-connected inverter for electric vehicles and renewable energy systems.

Junsung Park received the B.S. and M.S. degrees from the Seoul National University of Science and Technology, Seoul, Korea, in 2009 and 2011, respectively, where he is currently working toward the Ph.D. degree at the Power Electronics and Fuel Cell power Conditioning Laboratory.

His research interests include high-power dc–dc converter for electric vehicles and renewable energy systems.

Sewan Choi (S'92–M'96–SM'04) received the B.S. degree in electronic engineering from Inha University, Incheon, Korea, in 1985, and the M.S. and Ph.D. degrees in electrical engineering from Texas A&M University, College Station, TX, USA, in 1992 and 1995, respectively.

From 1985 to 1990, he was with Daewoo Heavy Industries as a Research Engineer. From 1996 to 1997, he was a Principal Research Engineer at Samsung Electro-Mechanics Co., Korea. In 1997, he joined the Department of Electrical and Information Engineering, Seoul National University of Science and Technology, Seoul, Korea, where he is currently a Professor. His research interests include power conversion technologies for renewable energy systems and dc–dc converters and battery chargers for electric vehicles.

Dr. Choi is an Associate Editor of the IEEE TRANSACTIONS ON POWER ELECTRONICS and the IEEE JOURNAL ON EMERGING AND SELECTED TOPICS IN POWER ELECTRONICS.